



Effect of micro-pin characteristics on flow and heat transfer by a circular jet impinging to the flat surface

Amirhosein Hadipour¹ · Mehran Rajabi Zargarabadi¹ · Maziar Dehghan²

Received: 9 September 2019 / Accepted: 23 December 2019 / Published online: 6 January 2020
© Akadémiai Kiadó, Budapest, Hungary 2020

Abstract

The effects of micro-pin characteristics on flow and heat transfer of a circular impinging jet are studied both experimentally and numerically. The studies are carried out for a single jet impinging ($D = 24$ mm) on a target plate that roughened by 48 micro-pins. The target surface is heated by a silicon rubber heater under a uniform heat flux of 2000 W m^{-2} . Two Re numbers (20,000 and 40,000), three distances between the pins and the jet ($S/D = 1$, $S/D = 2$, $S/D = 3$) and three nozzle-to-surface distance ratios (0.5, 1 and 2) are considered. Experimental and numerical results confirm that using micro-pin on the target surface has a significant effect on the distributions of Nusselt number. In addition, the results show that using the micro-pin on the target plate may result in both decrease and increase in the averaged Nusselt number depending on the arrangement of the micro-pins. For the Reynolds number of 40,000, the presence of the micro-pins at $S/D = 2.0$ can increase the average Nusselt number by 10.8%, 10.1% and 11% at $H/D = 0.5$, 1.0 and 2.0, respectively.

Keywords Impinging jet · Pin–fin surface · Heat transfer · Nusselt number

List of symbols

C_p Specific heat ($\text{N m kg}^{-1} \text{ K}^{-1}$)

d Pin diameter (mm)

D Nozzle diameter (mm)

H Nozzle-to-surface spacing (mm)

k Turbulence kinetic energy ($\text{m}^2 \text{ s}^{-2}$)

Nu Local Nusselt number

P Static pressure (Pa)

q'' Heat flux (W m^{-2})

Re Reynolds number

S The distance of pins to impingement point

R The target plate radius

T Temperature (K)

u Velocity (m s^{-1})

X Coordinates (x, y, s)

y^+ Dimensionless distance

μ Dynamic viscosity (N s m^{-2})

ρ Density (kg m^{-3})

Introduction

Jet impingement is classified as one of the most effective heat transfer techniques to/from a target surface, and it is widely used in different applications. Internal cooling of the gas turbine blade is one of the applications of the jet impingement wherein turbine blades expose to a gas stream with a high velocity and a high temperature. Hence, cooling the area of blades is much important to increase the turbine operation life. Previous studies on the jet impingement heat transfer were focused on many parameters such as the geometries of jet, jet-to-target distance and jet Reynolds numbers [1–4].

The impingement cooling for turbine blades and combustors can be more efficient with surface roughening elements. Wan et al. [5] numerically investigated the heat transfer characteristics of a jet impingement on a flat surface roughened with square pin–fins. Their numerical model was founded on the model presented by Spring et al. [6]. They tested four types of pin–fin configurations, a large pin–fin as well as a small pin–fin both located in an inline or staggered arrangement. They

✉ Mehran Rajabi Zargarabadi
rajabi@semnan.ac.ir

¹ Department of Mechanical Engineering, Semnan University,
P.O.B. 35131-191 Semnan, Iran

² Department of Energy, Materials and Energy Research
Center (MERC), Karaj, Iran

showed that better heat transfer could be achieved by small pin. Tingzhen et al. [7] proposed the combination of jet impingement, dimples and micro-channel heat sink to improve the heat transfer rate from a surface with constant heat flux. They concluded that when the dimple radius is large, micro-channel heat sink with impinging jets and dimples with larger dimples could show better heat transfer performance. In another study, Tingzhen et al. [8] investigated the influences of dimple height and arrangement. They found that optimal heat transfer could be achieved with large dimples. Huang et al. [9] studied jet impingement heat transfer enhancement on a micro-channel heat sink with dimples. Their results showed that MIJs with convex dimples have a good cooling performance. Teuscher et al. [10] investigated cooling by jet impingement with extended surfaces. Their results revealed a dependence of the thermal resistance on the flow rate. Xie et al. [11] investigated the effect of dimples/pins/protrusions/on the cooling performance of jet impingement for turbine blades at high Reynolds numbers.

Umair and Gulhane [12] performed a numerical investigation on heat transfer enhancement through pin–fin heat sinks by jet impingement. They showed that using the pin–fin interrupts the development of hydrodynamic and thermal boundary layers of the flow. Varun et al. [13] experimentally studied jet impingement on transverse and inclined discrete ribs. They found that combined geometries increase the heat transfer rate compared to the simple and single roughened geometry. Xie et al. [14] studied the heat transfer and friction performance for turbine blades with combined pin–fin/dimple/protrusion structure. They observed that the area-averaged Nusselt number for pin–fin/dimple/protrusion surface can increase by 31.2–127.3%. Brakmann et al. [15] analyzed an array of jet impingement on cubic micro-pin–fins surface both experimentally and numerically. They found that applying cubic micro-pin–fin on a flat surface can increase the heat flux for the surface to about 134–142%, with no extra pressure loss more than 14%.

Kim et al. [16] investigated the effects of pin spacing on the local heat transfer for multilayered jet impingement and effusion cooling. They found that increasing the number of pins results in better cooling performance. Trabold and Obot [17] studied the effect of jet-to-plate spacing and square ribs height. They found that ribs can be used for compensating the jet deflection in a high crossflow. Ndao et al. [18] analyzed the heat transfer enhancement from micro-pin–fins subjected to an impinging jet and concluded that the surface heat transfer coefficient increases considerably by using the micro-pin–fins. Wan et al. [19] studied the heat transfer rate of a jet impinging on square pin–fin surfaces and found

that the heat transfer rate can increase up to about 34.5% higher than the smooth surface.

Quan et al. [20] achieved an overall cooling effectiveness higher than 0.8 for a jet impinging on a pin–fin surface. Son et al. [21] and Yamawaki et al. [22] studied the cooling system by jet impingement with circular pin–fin surface. They found that the flat surface wetted area-averaged Nusselt number was higher than the pin–fin surface. However, for the pin–fin surface, the maximum pressure loss and total heat transfer rate increase up to 10% and 50%, respectively. Azad et al. [23] investigated the effects of the pin-finned plate heat transfer features for an impinging jet system. They showed that heat transfer of the pin-finned plate may decrease or increase the heat transfer rate depending on the air jet direction. Chyu et al. [24, 25] revealed that the pin height-to-diameter ratio and fin cross-sectional shape are important parameters concerning the friction factor and heat transfer coefficients. Sharif and Mothe [26] applied different turbulence models to simulate the impingement heat transfer. They observed that RSM has relatively better performance in reproducing the flow characteristics. Hong et al. [27] investigated the heat transfer in a jet impingement system with pin–fins. They found that the pin–fins increase the local heat transfer. Teuscher et al. [10] investigated impingement system cooling with extended surfaces and showed that parallel plate fins resulted in a decrease in the thermal resistance by a factor of 3.3–5.5. Xing et al. [28] conducted the experimental and numerical studies of heat transfer by jet impingement system on a smooth plate, a surface with rib and micro-rib roughened plate. They found that the highest augmentation of the overall averaged Nusselt number can be achieved on the micro-rib surface and the rib roughened plate.

According to the literature review, major improvements to the impingement heat transfer rates are possible by using roughened target surfaces such as pins, ribs or dimples. Pins intensify the turbulence and are used in the internal flow for improved heat transfer because they break the development of boundary layer and cause flow reattachment. The present study focused on experimental and numerical analyses on heat transfer from impinging jet on a pin–fin surface. The present study aims to present the important characteristics of the heat transfer from the impinging jet to the pin–fin surface. The circular pins with identical radius have been located around the impingement point in circular arrangement. The results of the pinned surface have been compared with the smooth surface. The effects of pin–fin on heat transfer and flow were studied considering governing parameters such as Reynolds numbers (20,000 and

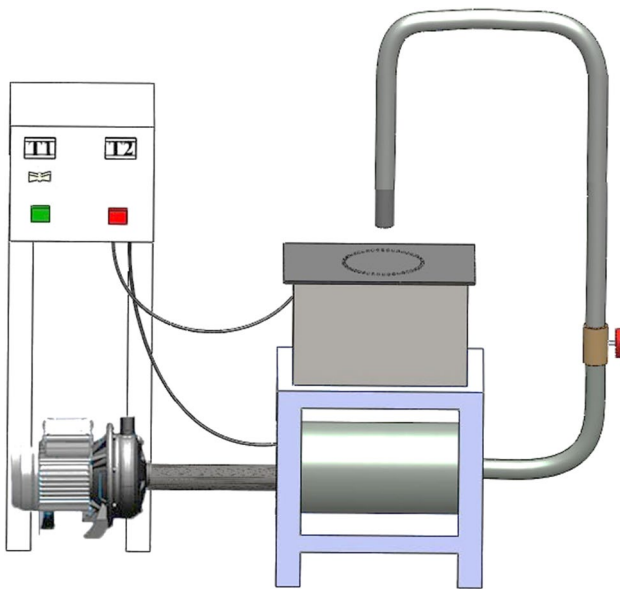


Fig. 1 Experimental setup: **a** the schematic of the test rig, **b** high-pressure fan and reservoir tank

Table 1 Uncertainties of experimental data

Equipment	Measuring errors
K-type thermocouple	± 0.4 T
Infrared camera	$\pm(2.2 + 2.5\% \text{ rdg})$
Hot wire	$\pm(0.1 + 1.0\% \text{ F.S})$
Pitot tube	$\pm 0.3\% \text{ F.S}$
Power supply	$\pm 1.5\% \text{ F.S}$

40,000), nozzle-to-plate spacing ($H/D = 0.5, 1$ and 2) and pin-to-injection point spacing ($S/D = 1, 2$ and 3).

Experimental

Experimental setup

The cooling system in the present study is shown in Fig. 1. The equipment consists of a high-pressure fan, control box, reservoir, temperature sensors, infrared camera, flow control valve and the flat plate subjected to a constant heat flux. The cooling airflow is supplied by a high-pressure fan which passes through a small reservoir tank. The length of the pipe is considered 25 times the jet diameter to ensure fully developed flow conditions at the jet exit. A ball valve is used to control the airflow rate for providing the desired Reynolds number. The airflow velocity is measured by a calibrated hot wire placed at

the center of the jet nozzle and just after the exit. The jet Reynolds number is calculated based on the averaged air velocity of the jet. The velocity profile has been measured by a Pitot tube with a micro-manometer. The uncertainty of the experimental results is presented in Table 1. The uncertainty of the calculated Nusselt number is less than $\pm 7.3\%$ according to the method of Kline and McClinton [29].

Data processing

These experiment and numerical analyses have been proposed to estimate the distribution of Nusselt number over the pin–fin surface for various jet Reynolds numbers and different pin-to-injection point distances. The tests are performed for three pin-to-injection point distances ($S/D = 1, 2$ and 3), two jet Reynolds numbers (20,000 and 40,000) and three nozzle-to-plate distance (H/D) of 0.5, 1 and 2. In all experiments, the local temperatures and the jet velocity have been measured at the steady-state condition. To examine the repeatability of the experiments as well as the results, each experiment is repeated 4 times. The difference between the two sets of measurements is found to be less than $\pm 3\%$.

Test section

In the present study, the heat transfer from a round jet impinging on pin–fin and smooth surfaces for different pin-to-injection point distances and Reynolds numbers is examined. For this purpose, a pin–fin surface with dimensions $300 \times 200 \times 2$ mm with cylindrical micro-pins with a diameter of 1 mm and height of 0.5 mm is used. In this study, the micro-pin surface is machined out of a metal block by material removal to create the inter-pin spaces. Micro-pin surface is manufactured by gang saw cutting on a computer numerical control (CNC) machine. The gang saw consists of multiple saw cutters on an arbor with precise spacing, which depends on the micro-pin surface geometry to be machined. The circular pins with identical radius are located in a circular arrangement around the injection point at the angle of 7.5° from each other as shown in Fig. 2. The circular air jet with 24 mm diameter ensures a fully developed flow at two Reynolds numbers of 20,000 and 40,000.

The main parts of the test plate are a stainless steel plate, a silicon heater, rock-wool insulation, plexiglass insulation and a stainless steel plate, as shown in Fig. 3. A silicone heater with a thickness of less than 3 mm is placed at the bottom of the target plate to provide a constant heat flux of 2000 W m^{-2} .

Fig. 2 **a** Schematic of the components of the target micro-pin surface. **b** The real configuration of the target micro-pin surface with 48 pins

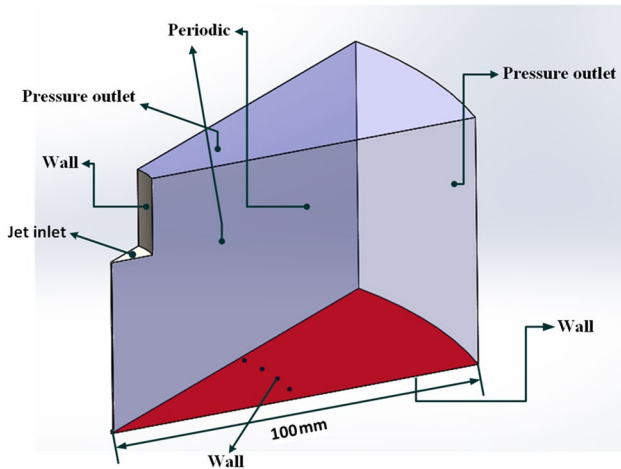
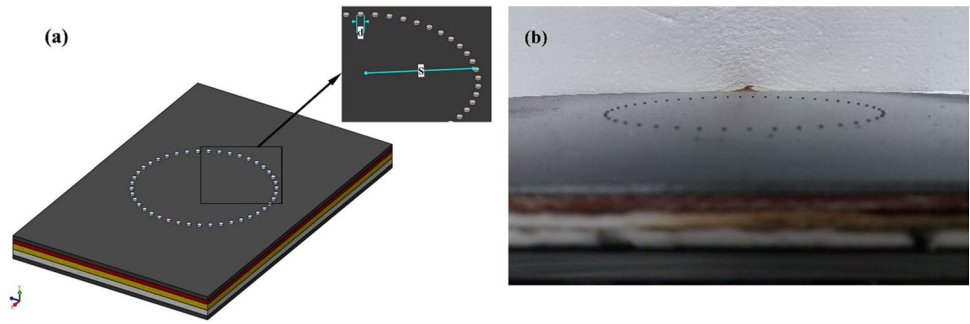


Fig. 3 The schematic of the boundary conditions

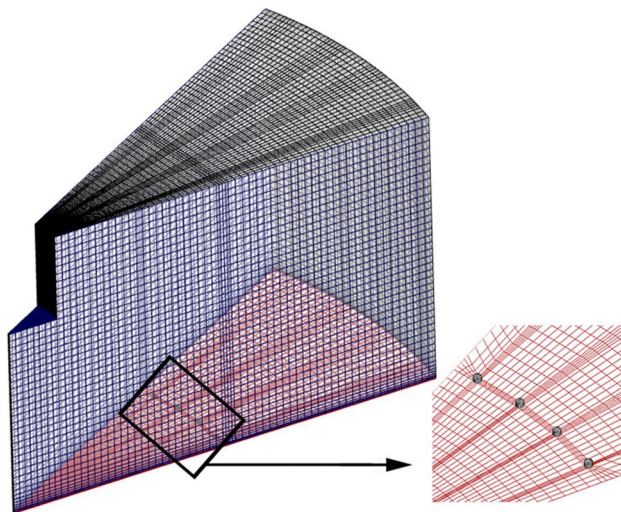


Fig. 4 Mesh distribution for the computational domain

The surface temperature distribution has been measured by an infrared camera. The target surface has been coated by a high emissivity black paint to enable temperature

measurement by the thermal camera. So, the local Nusselt number can be calculated by the following relation:

$$Nu = \frac{q''}{T_s - T_{jet}} \frac{D_{jet}}{k} \tag{1}$$

Numerical study

Computational domain

Figure 4 shows the computational domain and boundary conditions of the present study. In this study, two jet Reynolds numbers of 20,000 and 40,000 have been considered. The working fluid in this study is air at the ambient temperature and pressure. The air is incompressible, and the outlet boundary condition is the atmospheric pressure.

Solution method

3D Navier–Stokes equations (Eqs. 2–4), namely the continuity equation, momentum equation and energy equation, are solved by adopting the second-order upwind scheme used for the spatial discretization. The coupled algorithm has been used for pressure–velocity coupling [30].

$$\frac{\partial(\rho u_i)}{\partial x_i} = 0 \tag{2}$$

$$\frac{\partial}{\partial x_j}(\rho u_i u_j) = -\frac{\partial P}{\partial x_i} + \frac{\partial}{\partial x_j} \left(2\mu S_{ij} - \rho \overline{u'_i u'_j} \right) \tag{3}$$

$$\frac{\partial}{\partial x_j}(\rho C_p u_i T) = -\frac{\partial P}{\partial x_i} + \frac{\partial}{\partial x_i} \left(k \frac{\partial T}{\partial x_i} - \rho C_p \overline{u'_i T'} \right) \tag{4}$$

where u_i is the average velocity, u'_i, u'_j are turbulent components of the velocity and P is the static pressure. In Eq. (2), S_{ij} is the mean strain rate tensor:

$$S_{ij} = \frac{1}{2} \left(\frac{\partial u_i}{\partial x_j} + \frac{\partial u_j}{\partial x_i} \right) \tag{5}$$

The Reynolds stress and turbulent heat convection transfer are modeled using the SST $k-\omega$ with the enhanced wall treatment [31]. It is reported that the SST $k-\omega$ turbulence model gives more realistic results for impinging jet heat transfer with much less computational efforts compared to other RANS models [31].

Due to the capability of $k-\omega$ Wilcox model for predicting flow near walls and that of $k-\epsilon$ standard model for free flow far from walls, Menter [32] introduced a model based on the combination of these two models, which was called $k-\omega$ SST to capture the capabilities of both. Equations (6) and (7) are related to transport equations of k and ω , respectively:

$$\frac{\partial}{\partial x_i} (\rho u_i k) = \frac{\partial}{\partial x_j} \left[\left(\mu + \frac{\mu_t}{\sigma_k} \right) \frac{\partial k}{\partial x_j} \right] + \gamma \mu_t S^2 - \beta^* \rho k \omega \tag{6}$$

$$\begin{aligned} \frac{\partial}{\partial x_i} (\rho u_i \omega) = & \alpha \rho S^2 - \beta \rho \omega^2 + \frac{\partial}{\partial x_j} \left[\left(\mu + \frac{\mu_t}{\sigma_\omega} \right) \frac{\partial \omega}{\partial x_j} \right] \\ & + 2\rho(1 - F_1) \frac{1}{\omega \sigma_{\omega^2}} \frac{\partial k}{\partial x_j} \frac{\partial \omega}{\partial x_j} \end{aligned} \tag{7}$$

To complete the specification of the problem, the transport equation for intermittency γ is written as:

$$\frac{\partial}{\partial x_j} (\rho u_j \gamma) = F_\gamma - E_\gamma + \frac{\partial}{\partial x_j} \left[\left(\mu + \frac{\mu_t}{\sigma_\gamma} \right) \frac{\partial \gamma}{\partial x_j} \right] \tag{8}$$

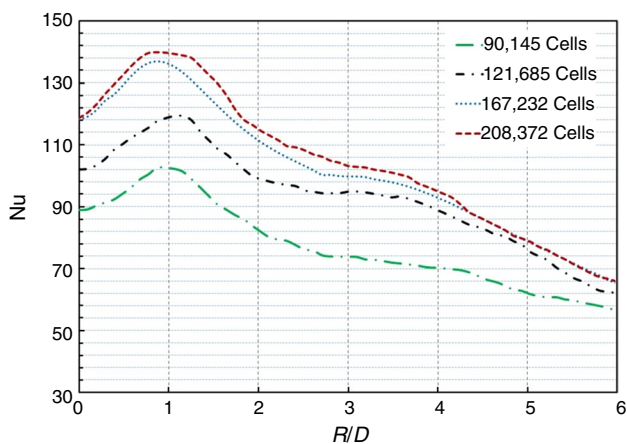


Fig. 5 Mesh-independency check for pin surface at Re = 20,000

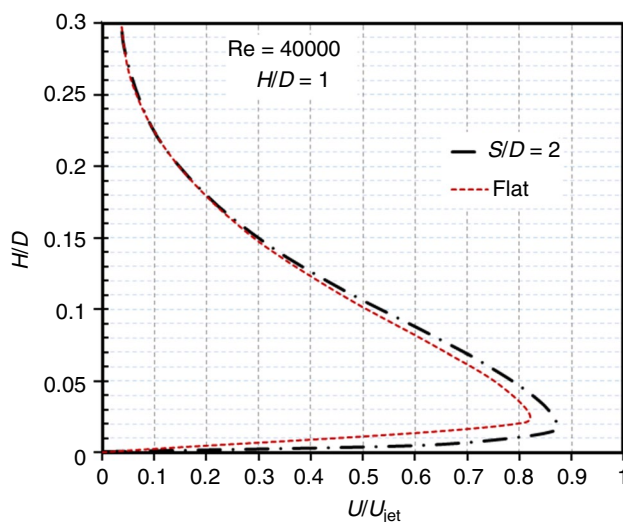


Fig. 6 Effects of using a row of micro-pin on velocity profile along vertical direction

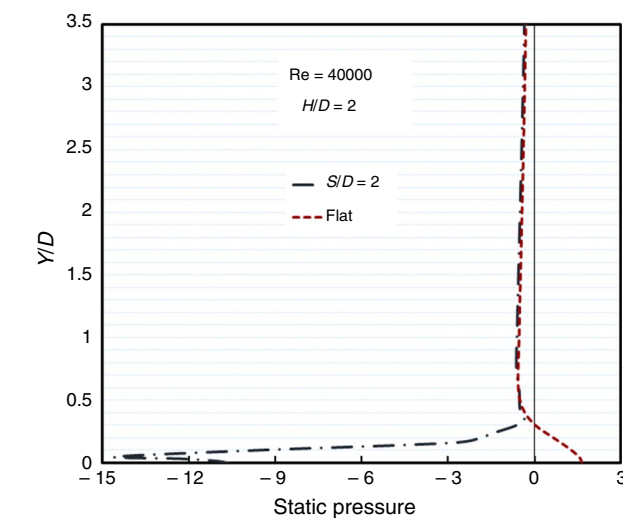
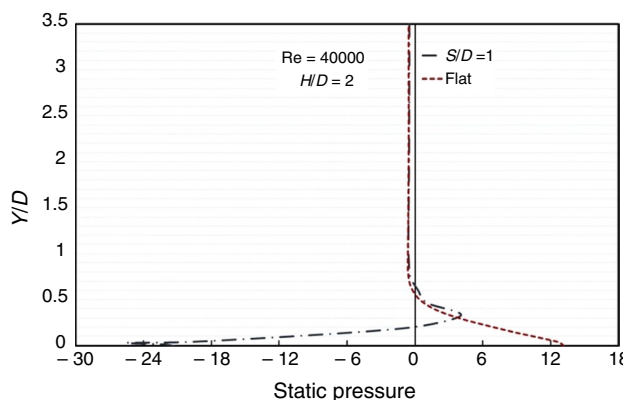


Fig. 7 Effects of micro-pin on the static pressure distribution along the vertical direction after the micro-pin position

Fig. 8 Effect of pin spacing from jet impingement location on the Nusselt number for $H/D = 1$: **a** $Re = 20,000$ and **b** $Re = 40,000$

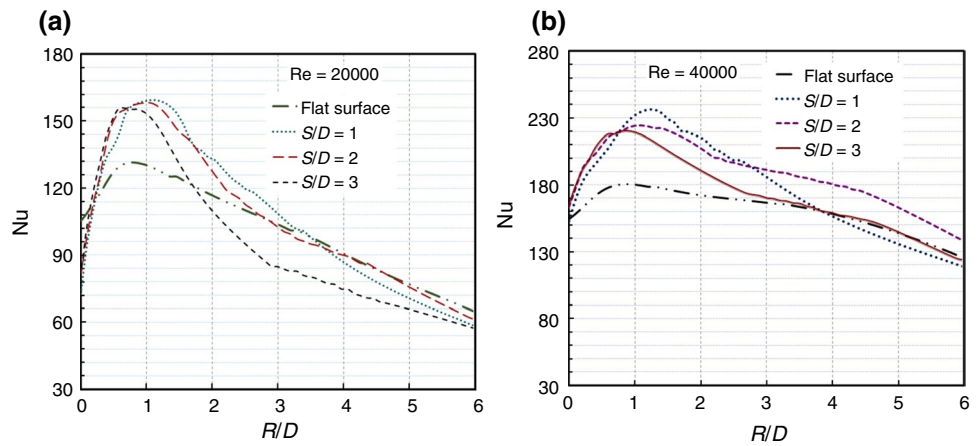


Table 2 Effect of micro-pin on area-averaged Nusselt number

H/D	Re	Smooth	$S/D = 1$	$S/D = 2$	$S/D = 3$
0.5	20,000	110.15	108.03	118.82	113.48
	40,000	184.87	183.11	204.99	198.34
1	20,000	85.84	81.12	88.56	82.87
	40,000	152.79	145.37	168.26	160.09
2	20,000	82.85	80.62	89.91	85.63
	40,000	145.57	144.39	161.63	151.30

The convergence of numerical simulation can be achieved when the root-mean-square residuals of all governing equations were less than 10^{-6} . The grid and the boundary condition for the numerical computations for the jet impingement system on the target surface (smooth and the pin–fin roughened plate) are shown in Fig. 4. The fine mesh with total number of 167,232 cells was used in the near-wall zone, which needs the dimensionless wall

distance of the first node y^+ to be about 0.5. Figure 5 shows the distribution of the Nusselt number for pin surface by $S/D = 2$ and $X/D = 2$ for four typical grid. As shown in Fig. 5 with the grid refinement from 167,232 to 208,372 cells, there are no significant changes in distribution Nusselt number.

Results and discussion

The effects of using a row of micro-pins around impingement place are studied under two following sections according to the thermal and flow structure features.

Flow structure

Figure 6 compares the velocity profiles for the smooth plate and the plate with the micro-pin ($S/D = 2$). It is seen that the dimensionless velocity distribution is affected due to the presence of the micro-pins. The velocity profile of the

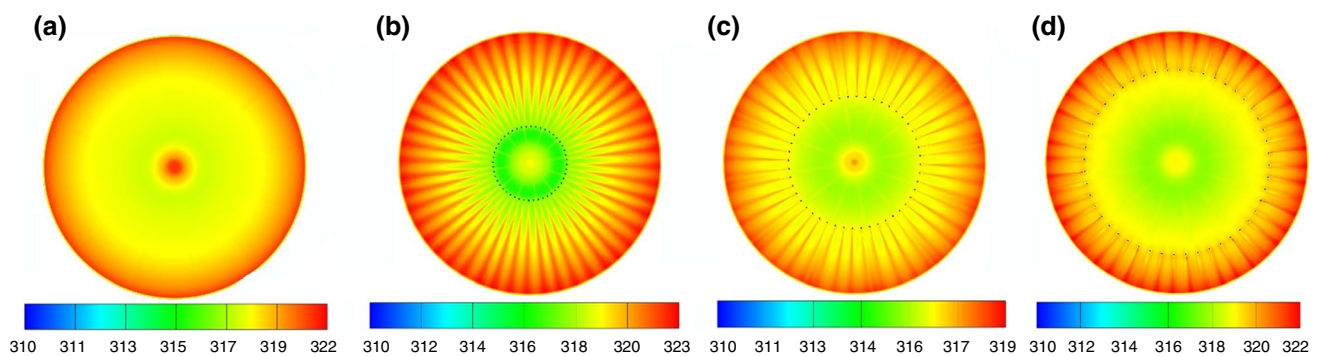


Fig. 9 Comparison of temperature (K) distributions at $Re = 40,000$ between the smooth plat **(a)** and micro-pinned surface, **b** $S/D = 1$ **c** $S/D = 2$ **d** $S/D = 3$

Table 3 Effect of micro-pin on the maximum temperature of the target plate at $H/D=1$

Re	Smooth (K)	$S/D=1$ (K)	$S/D=2$ (K)	$S/D=3$ (K)
20,000	330.4	333.1	329.5	334.8
40,000	321.1	322.4	319.1	321.8

pinned surface is similar to that of the smooth plate, but shows higher values than that of the smooth plate. This difference between the two velocities reaches its maximum in a near-wall region which would be the reason for having a higher Nusselt number for the pin surface compared to the smooth surface.

The effects of micro-pins on the static pressure distribution are shown in Fig. 7. The airflow passing over a micro-pin tends to separate and create a vortex flow in the downstream side of the micro-pin. The denser pin-fins on the target surface will highly contribute to the heat transfer quantity of the jet impingement system. The influence of the pins can be improved further by strategically rearranging each individual pin-fin.

Thermal performance

Figure 8 exhibits the effects of micro-pins location on the local Nusselt number. The pins are located in a circular arrangement with three different radiuses ($S/D=1, 2$ and 3). It can be seen that the Nusselt number is significantly affected by the location of pins. The local Nusselt number considerably increased in the impingement region ($R/D < 2.5$) by micro-pins with $S/D=2.0$. In addition, it can be found that the best position for micro-pins location is $S/D=2.0$ for both jet Reynolds numbers. As expected, the Nusselt number of roughened surfaces shows higher values than that of the smooth surface. In addition, roughening the surface with a row of micro-pin around the jet impingement point decreases the reduction rate of the Nusselt number away from the center.

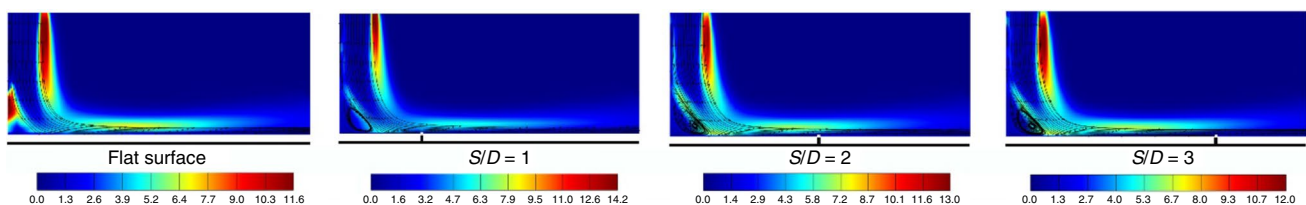
The effect of micro-pin on area-averaged Nusselt number is mentioned in Table 2. It can be concluded that the averaged Nusselt number significantly is affected by the location of pins. The results show that applying the micro-pins in location of $S/D=1$ decreases the average Nusselt number in all ranges of Re numbers and jet-to-surface distances of the present study. For the Reynolds number of 40,000, the presence of the micro-pins at $S/D=2.0$ can increase the average Nusselt number by 10.8%, 10.1% and 11% at $H/D=0.5, 1.0$ and 2.0 , respectively.

The temperature contours of the pinned surfaces are compared with the smooth surface in Fig. 9. It can be observed that applying the micro-pins at $S/D=1.0$ extends the high-temperature region on the target surface.

By moving the location of micro-pins to $S/D=2.0$ and 3.0 , the high-temperature region on the surface declines. Table 3 presents the effect of micro-pin on the maximum temperature at $H/D=1$. It can be observed that the minimum surface temperature can be achieved for applying the micro-pin at the location of $S/D=2.0$.

The turbulent kinetic energy contours at the x - y plate that crosses the pin are shown in Fig. 9. It can be seen that the highest turbulent kinetic energy belongs to the pinned plate with $S/D=1.0$. For this surface, the values of turbulent kinetic energy reduce dramatically downstream of the pins. Figure 10 shows that the presence of the pin at the location of $S/D=2.0$ increases the turbulent kinetic energy in both impingement and wall jet regions.

Figure 11 shows the experimental results as well as the numerical predictions, which are in a good agreement. As expected, both experimental and numerical results show that the Nusselt number increases by applying a row of micro-pin on the target plate compared to a flat surface, because of intensifying the turbulent structures and creating vortices. In addition, it is seen that the higher Re number corresponds to the higher Nusselt number for all nozzle-to-surface distances according to the previous studies [10, 11, 22, 27, 28]. Meanwhile, the accuracy of the experimental and numerical results is validated with the available data [33, 34] in Fig. 11.

**Fig. 10** Effect of location of micro-pins on turbulent kinetic energy distribution. $Re=20,000, H/D=1$

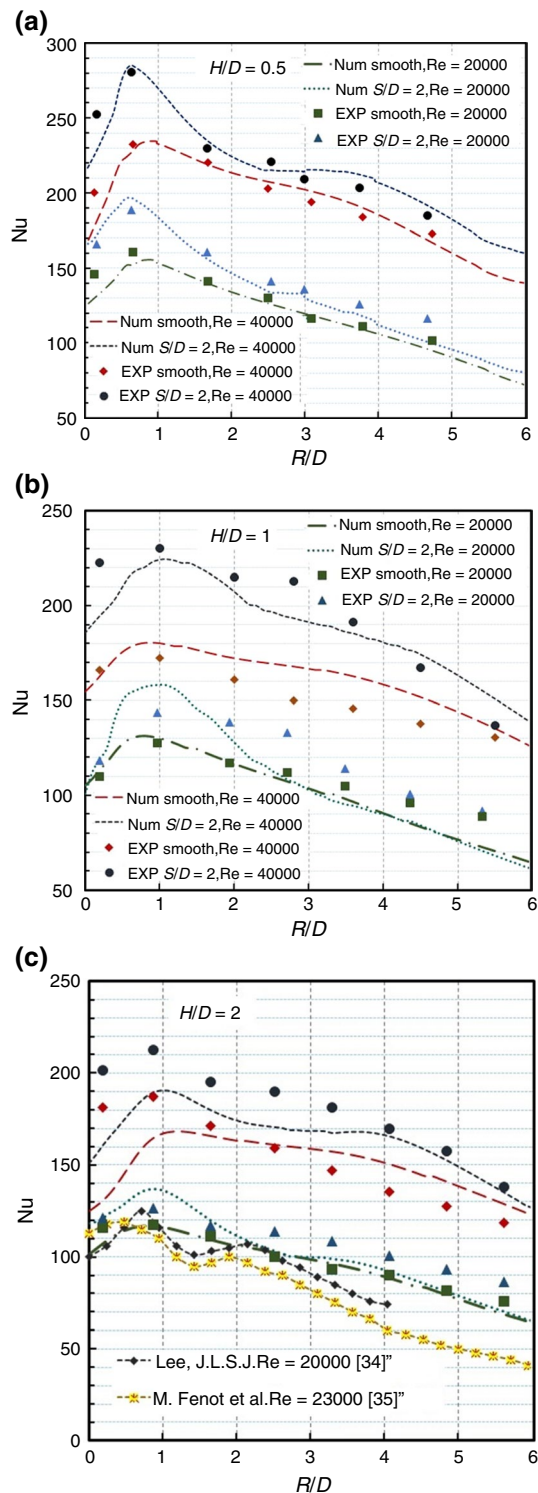


Fig. 11 Effects of the presence of a row of micro-pins on the Nu number for $S/D=2$ and for $Re=20,000$ and $40,000$: **a** $H/D=0.5$, **b** $H/D=1$ and **c** $H/D=2$

Conclusions

The thermal response, as well as the flow structure, of a flat circular plate under the target of an impinging jet in the presence/absence of micro-pins, was investigated both experimentally and numerically. The effect of location of the micro-pins, height of the jet and different jet stream velocities was studied under a constant heat flux thermal boundary condition. The highlights of the study are summarized as follows:

- Comparisons between numerical and experimental results confirm the applicability of the SST $k-\omega$ model in predicting the Nusselt number for impinging jets with micro-pin structures.
- Using a row of micro-pin around the impingement point on the target plate can increase the Nusselt number and heat transfer rate as well.
- Applying a row of pin-fin on the target plate also has a great influence on the flow field even by creating a negative zone of static pressure downstream of the micro-pins.
- The present study has shown that the location of the micro-fins has a noticeable influence on the temperature profile, especially the maximum temperature value to avoid hot spots. Hence, finding the optimum position of microstructures as well as the number of rows requires further comprehensive investigations.

References

1. Hong SK, Lee DH, Rhee DH, Cho HH. Local heat/mass transfer measurements on effusion plates in impingement/effusion cooling with rotation. *Int J Heat Mass Transf.* 2010;53(7):1373–9.
2. Hadipour A, Rajabi-Zargarabadi M. Heat transfer and flow characteristics of impinging jet on a concave surface at small nozzle to surface distances. *Appl Therm Eng.* 2018;138:534–41.
3. Rajabi Zargarabadi M, Rezaei E, Yousefi-Lafouraki B. Numerical analysis of turbulent flow and heat transfer of sinusoidal pulsed jet impinging on an asymmetrical concave surface. *Appl Therm Eng.* 2018;128:578–85.
4. Mohammadpour J, Rajabi-Zargarabadi M, Mujumdar AS, Ahmadi H. Effect of intermittent and sinusoidal pulsed flows on impingement heat transfer from a concave surface. *Int J Therm Sci.* 2014;76:118–27.
5. Wan C, Rao Y, Zhang X. Numerical investigation of impingement heat transfer on a flat and square pin-fin roughened plates. In: *ASME paper GT2013-94473* (2013).
6. Spring S, Xing Y, Weigand B. An experimental and numerical study of heat transfer from arrays of impinging jets with surface ribs. *ASME J Heat Transf.* 2012;134(8):082201.
7. Ming T, Cai C, Yang W, Shen W, Gan T. Optimization of dimples in microchannel heat sink with impinging jets—part A:

- mathematical model and the influence of dimple radius. *J Therm Sci.* 2018;27(3):195–202.
8. Ming T, Cai C, Yang W, Shen W, Feng W, Zhou N. Optimization of dimples in microchannel heat sink with impinging jets—part B: the influences of dimple height and arrangement. *J Therm Sci.* 2018;27(4):1–10.
 9. Huang X, Yang W, Ming T, Shen W, Yu X. Heat transfer enhancement on a microchannel heat sink with impinging jets and dimples. *Int J Heat Mass Transf.* 2017;112:113–24.
 10. Teuscher KL, Ramadhyani S, Incropera FP. Jet impingement cooling of an array of discrete heat sources with extended surfaces. *Enhanc Cool Tech Electron Appl HTD.* 1993;263:1–10.
 11. Xie GN, Sundén B, Zhang WH. Comparisons of pins/dimples/protrusions cooling concepts for a turbine blade tip-wall at high Reynolds numbers. *J Heat Transf.* 2011;133(6):061902.
 12. Umair SM, Gulhane NP. On numerical investigation of heat transfer augmentation through pin fin heat sink by laterally impinging air jet. *Proc Eng.* 2016;157:89–97.
 13. Varun RP, Saini SK, Singal, Investigation of thermal performance of solar air heater having roughness element as a combination of inclined and transverse ribs on the absorber plate. *Renew Energy.* 2008;33(6):1398–405.
 14. Xie Y, Shi D, Shen Z. Experimental and numerical investigation of heat transfer and friction performance for turbine blade tip cap with combined pin-fin-dimple/protrusion structure. *Int J Heat Mass Transf.* 2017;104:1120–34.
 15. Brakmann R, Chen L, Weigand B, Crawford M. Experimental and numerical heat transfer investigation of an impinging jet array on a target plate roughened by cubic micro pin fins. *J Turbomach.* 2016;138(11):111010.
 16. Kim SH, Ahn KH, Park JS, Jung EY, Hwang KY, Cho HH. Local heat and mass transfer measurements for multi-layered impingement/effusion cooling: effects of pin spacing on the impingement and effusion plate. *Int J Heat Mass Transf.* 2017;105:712–22.
 17. Trabold TA, Obot NT. Impingement heat transfer within arrays of circular jets: part II—effects of crossflow in the presence of roughness elements. *J Turbomach.* 1987;109(4):594–601.
 18. Ndao S, Lee HJ, Peles Y, Jensen MK. Heat transfer enhancement from micro pin fins subjected to an impinging jet. *Int J Heat Mass Transf.* 2012;55(1–3):413–21.
 19. Wan C, Rao Y, Chen P. Numerical predictions of jet impingement heat transfer on square pin-fin roughened plates. *Appl Therm Eng.* 2015;80:301–9.
 20. Quan D, Liu S, Li J, Liu G. Investigation on cooling performance of impingement cooling devices combined with pins. In: *ASME turbo expo*, pp 793–799 (2005).
 21. Son C, Dailey G, Ireland P, Gillespie D. An investigation of the application of roughness elements to enhance heat transfer in an impingement cooling system. In: *ASME GT2005e68504*.
 22. Yamawaki S, Nakamata C, Imai R, Matsuno S, Yoshida T, Mimura F, Kumada M. Cooling performance of an integrated impingement and pin fin cooling configuration. In: *ASME GT2003e38215*.
 23. Azad GS, Huang Y, Han JC. Jet impingement heat transfer on pinned surfaces using a transient liquid crystal technique. *J Thermophys Heat Transf.* 2000;14(2):186–93.
 24. Chyu MK. Heat transfer and pressure drop for short pin-fin arrays with pin endwall fillet. *ASME J Heat Transf.* 1990;112:926–32.
 25. Chyu MK, Hsing YC, Shih TIP, Natarajan V. Heat transfer contributions of pins and endwall in pin-fin arrays: effects of thermal boundary condition modeling. *ASME J Turbomach.* 1999;121:257–63.
 26. Sharif MAR, Mothe KK. Parametric study of turbulent slot-jet impingement heat transfer from concave cylindrical surfaces. *Int J Therm Sci.* 2010;49:428–42.
 27. Hong SK, Rhee DH, Cho HH. Heat/mass transfer with circular pin fins in impingement/effusion cooling system with crossflow. *AIAA J Thermophys Heat Transf.* 2006;20(4):728–37.
 28. Xing Y, Spring S, Weigand B. Experimental and numerical investigation of impingement heat transfer on a flat and micro-rib roughened plate with different crossflow schemes. *Int J Therm Sci.* 2011;50:1293–307.
 29. Kline SJ, McClintock FA. Describing uncertainties in single-sample experiments. *J Mech Eng.* 1953;75:3–8.
 30. Latimer BR, Pollard A. Comparison of pressure-velocity coupling solution algorithms. *Numer Heat Transf.* 1985;8(6):635–52.
 31. Yakhot V, Orszag SA. Development of turbulence models for shear flows by double expansion technique. *J Phys Fluid.* 1991;4:1510–20.
 32. Menter FR. Two equation eddy-viscosity turbulence models for engineering application. *AIAA J.* 1994;32(8):269–89.
 33. Lee JLSJ. Stagnation region heat transfer of a turbulent axisymmetric jet impingement. *Exp Heat Transf.* 1999;12(2):137–56.
 34. Fénot M, Vullierme JJ, Dorignac E. Local heat transfer due to several configurations of circular air jets impinging on a flat plate with and without semi-confinement. *Int J Therm Sci.* 2005;44(7):665–75.

Publisher's Note Springer Nature remains neutral with regard to jurisdictional claims in published maps and institutional affiliations.